Dyes and Pigments 88 (2011) 307–314

Contents lists available at ScienceDirect

Dyes and Pigments

journal homepage: www.elsevier.com/locate/dyepig

N-Heteroaryl-1,8-naphthalimide fluorescent sensor for water: Molecular design, synthesis and properties

Zhiwei Li, Qiwu Yang, Ruixiang Chang, Guochun Ma, Mingxi Chen, Wenqin Zhang*

Department of Chemistry, School of Sciences, Tianjin University, Tianjin 300072, PR China

ARTICLE INFO

Article history:
Received 25 June 2010
Received in revised form
26 July 2010
Accepted 27 July 2010
Available online 5 August 2010

Keywords:
N-heteroaryl-1,8-naphthalimide
Solvent effect
DFT
Fluorescent sensor
Stern–Volmer equation
Water content

ABSTRACT

A series of *N*-heteroaryl-1,8-naphthalimides with good sensitivity to solvent polarity were prepared. Empirical and quantum calculations showed that the electron withdrawing effect of the heteroaryl group increases the change in dipole moment on excitation which results in the fluorescence quantum yield dramatically falling as the solvent polarity increases. A typical compound 4-(1-piperidyl)-*N*-(2-pyrimidinyl)-1,8-naphthalimide was chosen to determine the water content in six common solvents (*p*-dioxane, tetrahydrofuran, acetone, dimethylformamide, acetonitrile and methanol). Fluorescence intensity changes as a function of water content correlated well with a modified Stern–Volmer equation over a wide range, with detection limits being 0.016% and 0.020% for acetone and tetrahydrofuran, respectively.

1. Introduction

The detection and quantification of water content in organic solvents is of great significance in routine chemical analysis and has many practical applications in industrial processes.[1,2] Many analytical approaches and techniques have been established for the determination of water in a wide variety of organic solvents. In addition to the well established Karl Fischer method [3,4], chromatographic methods [5], electrochemical methods based on impedance [6], conductance [7], and amperometry [8,9] as well as spectroscopic techniques [10,11] have been used to detect water content and humidity.

Among the various systems available for water detection, fluorescence-based sensors have drawn considerable attention owing to their high sensitivity and reasonable selectivity. The most widely used fluorescent sensors for water detection are based on fluorescence intensity which is simple to measure. Suzuki's group [12] synthesized three fluorescent acridinyl indicators for sensing water content in organic solvents, and one of them was covalently immobilized to a hydrophilic membrane. These sensors enable the continuous monitoring of water content in a flow-through system. Another sensing membrane system was prepared by copolymerizing a chalcone derivative on a glass slide, and it showed even better analytical performance for detecting water [13]. Ooyama et al. [14,15] designed a novel fluorescent PET (Photoinduced Electron Transfer) sensor for proton and water detection, based on phenylaminonaphtho[1,2-d]oxazol-2-yl-type fluorophores. Chang and coworkers recently prepared several fluorescence water sensors based on an 8-hydroxyquinoline derivative [16], fluorescein [17] and a phenol-indole dye [18]. Luminescent nanospheres fabricated using an europium cation, $Eu(TTA)_3phen$, have also been employed to test for trace amounts of water in ethanol [19].

Wavelength and fluorescence life-time based measurements have also been developed to detect water. Li et al. used a fluorescent anionic $Pb_4Br_{11}^{3-}$ cluster to determine micro water content in aprotic solvents by measuring the Stokes shift [20]. Fluorescence life-time based sensors for water, which contain fluorescent metal–ligand compounds (Rudppz [1] or $[Os(dppz)(dppe)_2](PF_6)_2$ [2]) have been described, however, their complexity and the rigorous demands on instrumentation restrict their wide application.

Currently, the design of novel fluorescent sensors for water continues to be an exciting area of research. The most important step in developing a water sensor is the choice of an indicator, which displays water induced changes in its photophysical properties. This work focuses on the use of 4-aminonaphthalimide derivatives as suitable fluorophores for water sensing.

The absorption and fluorescence properties of 4-aminonaphthalimide derivatives have been extensively studied [21–25].

* Corresponding author. Tel.: +86 22 27890922; fax: +86 22 27403475.
E-mail address: zhangwenqin@tju.edu.cn (W. Zhang).

0143-7208/$ – see front matter © 2010 Elsevier Ltd. All rights reserved.
doi:10.1016/j.dyepig.2010.07.009

Most of these compounds are sensitive to their surroundings and their spectral properties are usually affected by the nature of the solvent. Generally for 4-aminonaphthalimide, the fluorescence quantum yield decreases with an increase in solvent polarity.

Quite recently related work has been published by Niu and co-workers. *N*-amino-4-(2-hydroxyethylamino)-1,8-naphthalimide was synthesized as a fluorescence probe for determining water content in dioxane, acetonitrile and ethanol [26]. Niu et al. also synthesized two 1,8-naphthalimide fluorescence indicators for use in the fabrication of sensing membranes for water detection in organic solvents [27,28]. However the linear response of these membranes to water was relatively low. In this work, the intramolecular charge transfer (ICT) upon excitation of the naphthalimide ring was enhanced by the introduction of a heteroaryl moiety with electron deficient properties to naphthalimide. The afforded compounds, 4-(1-piperidyl)-*N*-heteroaryl-1,8-naphthalimides, were found to have the highest sensitivity to the polarity of the surrounding solvent, which make these compounds useful as polarity probes.

2. Experimental

2.1. Materials and measurements

All chemicals and solvents used in the synthesis were of analytical grade and used without further purification. The solvents for spectral analysis were purchased as spectrophotometric grade and dried by standard methods before use. Double distilled water was used throughout the work. Melting points were taken on a Yanagimoto MP-500 apparatus and are uncorrected. FT-IR spectra were collected with a BIO-RAD FTS 3000 Infrared Spectrometer. ^{1}H and ^{13}C NMR spectra were recorded on a Varian Oxford 500 (500 MHz) instrument using TMS as the internal standard and MS were recorded on a LCQ electron spray mass spectrometer (ESMS, Finnigan). UV spectra were recorded on a HP 8453 UV–Visible spectrophotometer and fluorescent spectra were collected on a Varian Cary Eclipse spectrometer.

The sample solutions containing different amounts of water in pure organic solvents were freshly prepared prior to measurement according to the following procedures: Standard solutions containing 2.0% (v/v) and 10% (v/v) H_2O in dry solvents were firstly prepared. A probe stock solution was also prepared in the same dry solvent (1.0×10^{-4} mol L^{-1}). A micropipette was used to add aliquots of each of the above solution to a 10-mL volumetric flask. The solution was then diluted with a dry solvent to give the required probe concentration as well as the desired water content between 0 and 5.0%. For working solutions containing more than 5.0% H_2O, the water and dry solvent were added directly to the volumetric flask before the appropriate dilution.

The fluorescence quantum yields of the sample solutions were measured using quinine sulfate as the reference compound ($\Phi_f = 0.546$ in 1 N H_2SO_4) [29].

2.2. Computational details

The structure of 1,8-naphthalimide derivatives was optimized by density functional theory (DFT) using the Becke3LYP [30–33] (B3LYP) functional. The geometry of the first excited state was fully optimized using configuration interactions involving single excited configurations (CIS) [34], and electronic properties and orbitals of the excited states were performed using Time-dependent density functional theory (TD-DFT) [35–37], with the B3LYP functional (TD-B3LYP) and the 6-31 + G* basis set. All the calculations were performed with the GAUSSIAN 03 program [38].

2.3. Synthesis

The derivatives **3a**–**c** were synthesized following the two-step procedure indicated in Scheme 1.

2.3.1. General procedure for the synthesis of 4-bromo-N-heteroaryl-1,8-naphthalimide *2*

Method A: A mixture of 4-bromo-1,8-naphthalic anhydride **1** (1.97 g, 7 mmol) and a heteroaromatic amine (12 mmol) in 140 mL toluene was placed in a 250 mL round-bottom flask, equipped with a Dean-Stark trap and condenser. The reaction mixture was allowed to reflux for 15 h under a nitrogen atmosphere. After cooling to room temperature, the precipitate was collected by filtration, washed with water and dried under vacuum. The crude solid was recrystallized from xylene to give white or light yellow needles.

Method B: To an anhydrous toluene (50 mL) solution of 4-bromo-1,8-naphthalic anhydride **1** (500 mg, 1.8 mmol), $AlCl_3$ (480 mg, 3.6 mmol) was added Et_3N (910 mg, 9 mmol) and a heteroaromatic amine (3.6 mmol). The mixture was refluxed for 3 h under a nitrogen atmosphere. After cooling, the solvent was evaporated under reduced pressure and the solid product was filtered and washed successively with 3 mol L^{-1} HCl aqueous solution and water. After drying in air, the crude solid was recrystallized from xylene to give the desired pure product.

*2.3.1.1. 4-Bromo-N-(2-pyridyl)-1,8-naphthalimide (**2a**).* Mp: 258–260 °C [literature [39]: 265–269 °C]; IR (KBr) ν (cm^{-1}) 3084, 3063, 1713, 1672, 1368, 1243; ^{1}H NMR ($CDCl_3$) δ: 8.74–8.75 (m, 1H), 8.70 (dd, $J_1 = 7.3$ Hz, $J_2 = 1.1$ Hz, 1H), 8.64 (dd, $J_1 = 8.6$ Hz, $J_2 = 1.1$ Hz, 1H), 8.45 (d, $J = 7.9$ Hz, 1H), 8.07 (d, $J = 7.8$ Hz, 1H), 7.95 (td, $J_1 = 7.8$ Hz, $J_2 = 2.0$ Hz, 1H), 7.89 (dd, $J_1 = 8.5$ Hz, $J_2 = 7.3$ Hz, 1H), 7.45–7.48 (m, 1H), 7.41–7.42 (m, 1H).

*2.3.1.2. 4-Bromo-N-(2-thiazolyl)-1,8-naphthalimide (**2b**).* Mp: 296–297 °C; IR (KBr) ν (cm^{-1}) 3087, 1717, 1682, 1363, 1236; ^{1}H NMR ($CDCl_3$) δ: 8.72 (dd, $J_1 = 7.3$ Hz, $J_2 = 1.1$ Hz, 1H), 8.68 (dd, $J_1 = 8.5$ Hz, $J_2 = 1.1$ Hz, 1H), 8.48 (d, $J = 7.9$ Hz, 1H), 8.11 (d, $J = 7.9$ Hz, 1H), 7.94 (d, $J = 4.6$ Hz, 1H), 7.91 (dd, $J_1 = 8.5$ Hz, $J_2 = 7.3$ Hz, 1H), 7.62 (d, $J = 3.5$ Hz, 1H).

*2.3.1.3. 4-Bromo-N-(2-pyrimidinyl)-1,8-naphthalimide (**2c**).* Mp: 283–285 °C [literature [39]: 277–279 °C]; IR (KBr) ν (cm^{-1}) 3084, 3053, 1712, 1672, 1401, 1371, 1249; ^{1}H NMR ($CDCl_3$) δ: 9.07 (d, $J = 4.9$ Hz, 2H), 8.58 (d, $J = 7.7$ Hz, 2H), 8.34 (d, $J = 7.8$ Hz, 1H), 8.23 (d, $J = 7.9$ Hz, 1H), 8.02 (t, $J = 7.9$ Hz, 1H), 7.74 (t, $J = 4.9$ Hz, 1H).

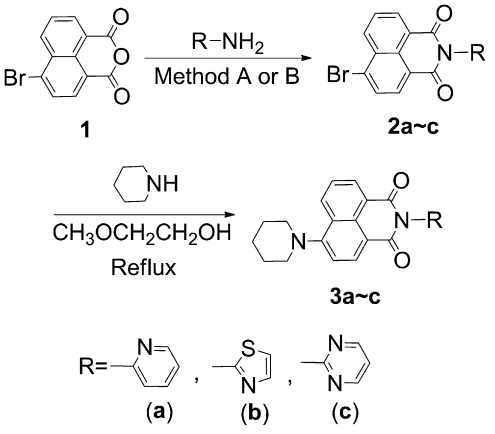

Scheme 1. Synthesis of 4-(1-piperidyl)-*N*-heteroaryl-1,8-naphthalimides.

*2.3.2. General procedure for the synthesis of 4-(1-piperidyl)-N-heteroaryl-1,8-naphthalimide **3***

A mixture of 4-bromo-*N*-heteroaryl-1,8-naphthalimide **2** (1.5 mmol) and piperidine (1.28 g, 15 mmol) in 20 mL ethylene glycol monomethyl ether was refluxed for 9 h under N_2. After reaction, the solvent was evaporated under vacuum and the resulting solid was recrystallized from xylene to give **3** as orange crystals.

*2.3.2.1. 4-(1-Piperidyl)-N-(2-pyridyl)-1,8-naphthalimide (**3a**).* Yield: 60.6%; mp: 243–248 °C; IR (KBr) ν (cm^{-1}) 1700, 1656, 1586, 1368, 1271; ^{1}H NMR ($CDCl_3$) δ: 8.73–8.74 (m, 1H), 8.61 (dd, J_1 = 7.2 Hz, J_2 = 1.2 Hz, 1H), 8.53 (d, J = 8.1 Hz, 1H), 8.45 (dd, J_1 = 8.5 Hz, J_2 = 1.2 Hz, 1H), 7.92 (td, J_1 = 7.7 Hz, J_2 = 1.9 Hz, 1H), 7.70 (dd, J_1 = 8.5 Hz, J_2 = 7.3 Hz, 1H), 7.39–7.44 (m, 2H), 7.20 (d, J = 8.1 Hz, 1H), 3.27 (t, J = 5.0 Hz, 4H), 1.88–1.93 (m, 4H), 1.73–1.76 (m, 2H); ^{13}C NMR ($CDCl_3$) δ: 24.58, 26.45, 54.77, 114.99, 115.92, 123.37, 124.11, 124.51, 125.61, 126.61, 130.78, 131.41, 131.58, 133.26, 138.66, 150.17, 150.20, 157.97, 164.33, 164.88; ESI-MS (positive) *m/z* calcd: 357.41; found: 358.32 ($[M + H]^+$), 714.86 ($[2M]^+$), 737.03 ($[2M + Na]^+$).

*2.3.2.2. 4-(1-Piperidyl)-N-(2-thiazolyl)-1,8-naphthalimide (**3b**).* Yield: 49.0%; mp: 237–238 °C; IR (KBr) ν (cm^{-1}) 1704, 1663, 1585, 1350, 1233; ^{1}H NMR ($CDCl_3$) δ: 8.62 (d, J = 7.3 Hz, 1H), 8.54 (d, J = 8.2 Hz, 1H), 8.46 (d, J = 8.5 Hz, 1H), 7.92 (d, J = 3.6 Hz, 1H), 7.71 (t, J = 7.4 Hz, 1H), 7.58 (d, J = 3.5 Hz, 1H), 7.21 (d, J = 8.2 Hz, 1H), 3.28 (t, J = 4.9 Hz, 4H), 1.89–1.93 (m, 4H), 1.74–1.77 (m, 2H); ^{13}C NMR ($CDCl_3$) δ: 24.55, 26.41, 54.75, 115.03, 115.16, 122.50, 122.82, 125.65, 126.60, 130.78, 131.90, 132.02, 133.75, 141.48, 156.31, 158.35, 163.94, 164.59; ESI-MS (positive) *m/z* calcd: 363.43; found: 364.30 ($[M + H]^+$), 748.94 ($[2M + Na]^+$).

*2.3.2.3. 4-(1-Piperidyl)-N-(2-pyrimidinyl)-1,8-naphthalimide (**3c**).* Yield: 98.2%; mp: 246–248 °C; IR (KBr) ν (cm^{-1}) 1701, 1658, 1573, 1372, 1239; ^{1}H NMR ($CDCl_3$) δ: 8.98 (d, J = 5.0 Hz, 2H), 8.61 (d, J = 7.2 Hz, 1H), 8.53 (d, J = 8.1 Hz, 1H), 8.45 (d, J = 8.4 Hz, 1H), 7.71 (t, J = 7.8 Hz, 1H), 7.46 (t, J = 4.9 Hz, 1H), 7.20 (d, J = 8.1 Hz, 1H), 3.27 (t, J = 4.6 Hz, 4H), 1.88–1.93 (m, 4H), 1.74–1.76 (m, 2H); ^{13}C NMR ($CDCl_3$) δ: 24.57, 26.43, 29.93, 54.77, 114.97, 115.63, 121.13, 123.14, 125.58, 126.65, 130.88, 131.60, 133.28, 157.38, 158.11, 159.67, 164.01, 164.57; ESI-MS (positive) *m/z* calcd: 358.39; found: 358.31 ($[M]^+$), 359.27 ($[M + H]^+$), 716.83 ($[2M]^+$), 739.04 ($[2M + Na]^+$).

3. Result and discussion

3.1. Synthesis

Up to now, a large number of 1,8-naphthalimide derivatives have been synthesized, but studies of *N*-heteroaryl substituted 1,8-naphthalimides has been inadequate, especially for those containing electron deficient heterocycles. Cao et al. have synthesized a variety of substituted *N*-aryl and *N*-heteroaryl 1,8-naphthalimides [39]. The reactions were promoted by zinc acetate in pyridine, but the yields were not given. Moreover, in their experiments the products were purified by preparative layer chromatography, which would not be suitable for large-scale preparation.

In this paper, two new methods (A and B) were developed for the reaction of heteroaromatic amines with 4-bromo-1,8-naphthalic anhydride (Table 1). Method A was carried out under refluxing conditions in toluene, and N-heteroaryl substituted products were readily obtained by recrystallization in good yield. This procedure is simple and convenient, but a long reaction time is required. Moreover it failed to produce a product for 2-aminopyrimidine due to the electron deficient nature of the amino group. When an $AlCl_3/Et_3N$ pair was used as the promoter, **2c** was afforded after a short refluxing time (3 h) and a purified yield of 94.6%. Using the same method B, **2a** and **2b** were also obtained with improved yields compared to those of Method A.

Table 1
Synthesis of 4-bromo-*N*-heteroaryl-1,8-naphthalimide **2** using Method A and Method B.

Compound	R	Yield[a]	
		Method A[b]	Method B[c]
2a	2-pyridyl	81.3%	92.1%
2b	2-thiazolyl	75.6%	89.4%
2c	2-pyrimidinyl	nr	94.6%

[a] Isolated yields.
[b] The reactions were carried out under reflux for 15 h in toluene.
[c] The reactions were carried out under reflux for 3 h in toluene in the presence of $AlCl_3$ and Et_3N.

3.2. Spectral characteristics and corresponding mechanism

The absorption and fluorescence spectra of 4-(1-piperidyl)-*N*-heteroaryl-1,8-naphthalimides (**3**) were measured in various solvents with different polarities and the spectral data is presented in Table 2 and Table S1. For convenience, the solvents are arranged in order of increasing polarity using a widespread empirical scale of solvent polarity $E_T(30)$ (the molar electronic transition energy) [40]. Compounds **3a**, **3b** and **3c** all have similar spectral properties, and **3c** was selected as the representative compound to be more extensively investigated.

The absorption spectrum of **3c** exhibits a broad and structureless peak in all the examined solvents (Fig. S1A), which can be attributed to an intramolecular charge transfer (ICT) from the piperidyl group to the naphthalimide moiety. As expected for a typical charge-transfer transition, an increase in the solvent polarity leads to a bathochromic shift of the absorption maximum. The high extinction coefficients (ϵ from 11,500 to 13,200) suggest that the electronic transition from the ground state to the excited state has a $\pi-\pi^*$ character.

The effect of the polarity of the medium on the fluorescence is more pronounced than that on the absorption spectrum (Fig. S1B). This is because the ICT effect leads to a large dipole moment in the excited state. According to the Franck–Condon principle, the CT (charge transfer) emission spectrum is expected to show a much

Table 2
Photophysical properties of **3c** (1.0×10^{-5} mol L^{-1}) in various solvents[a].

Number	Solvent	E_T (30)	λ_A (nm)	log ε	λ_{em} (nm)	$\Delta\bar{\nu}$(cm^{-1})	Φ_f
	Gas-phase[b]		387 (f^c = 0.2571)		435 (f^c = 0.2914)		
1	Cyclohexane	31.2	389	4.07	469	4385	0.64
2	CCl_4	32.5	396	4.08	481	4463	0.61
3	Toluene	33.9	401	4.06	498	4857	0.58
4	*p*-Dioxane	36.0	401	4.07	508	5253	0.55
5	THF	37.4	402	4.11	515	5458	0.35
6	Ethyl acetate	38.1	400	4.09	516	5620	0.31
7	Chloroform	39.1	414	4.11	512	4623	0.60
8	Dichloromethane	41.1	415	4.11	522	4939	0.52
9	Acetone	42.2	408	4.09	531	5677	0.039
10	DMF	43.8	417	4.08	539	5428	0.005
11	DMSO	45.0	421	4.07	544	5371	0.004
12	Acetonitrile	46.0	413	4.11	540	5695	0.017
13	Methanol	55.5	420	4.12	544	5427	0.002

[a] Absorption wavelength (at the maximum absorption), λ_A; emission wavelength (at the maximum intensity), λ_{em}; Stokes shifts, $\Delta\bar{\nu}$; extinction coefficient, ε; fluorescence quantum yields, Φ_f.
[b] Calculated data from DFT.
[c] Oscillator strength.

stronger influence from the environment than the CT absorption spectrum does. A change of the solvent from cyclohexane to methanol leads to a red shift of the fluorescence maximum of **3c** by 75 nm. This magnitude of fluorescence shift is twice that of the absorption shift. This observation suggests that the excited state of **3c** is more polar than the ground state. Accordingly, in general, the Stokes shifts increases with increasing solvent polarity and the fluorescence quantum yields decrease dramatically. This phenomenon occurs because an increase in the medium polarity enhances the nonradiative deactivation of the fluorescent state of the molecule, which primarily depends on the nitrogen inversion rate of the amino group [22,25].

The heteroaryl substituted 4-(1-piperidyl)naphthalimide prepared in this work was found to have a much greater effect on the fluorescence quantum yield than previously prepared compounds with alkyl or aryl groups on the imide nitrogen (structures are given in Fig. 1). Saha and Samanta reported that the fluorescence quantum yields of 4-(1-piperidyl)-*N*-butyl-1,8-naphthalimide (**BNI**) in hexane and methanol are 0.76 and 0.01, respectively, i.e., a 76-fold change [22]. Mednykh et al. gave the fluorescence quantum yields of 4-(1-piperidyl)-*N*-phenyl-1,8-naphthalimide (**PNI**) in toluene and methanol as 0.65 and 0.12, respectively, about a 5-fold decrease [25]. However, the fluorescence quantum yield for **3c** in toluene and methanol decreases 290-folds, and the change from cyclohexane to methanol is up to 320-fold.

Considering the electron deficient property of pyrimidine, we propose that the electron withdrawing effect of the heteroaryl group increases the ICT in the excited state, which also enhances the dipole moment of 4-(1-piperidyl)naphthalimide. This causes the highest sensitivity of **3c** to solvent polarity compared to **BNI** and **PNI**. In order to demonstrate our hypothesis, it is necessary to estimate the change in the dipole moment from the ground state to the excited state ($\Delta\mu$).

The effect of solvent polarity can be studied in terms of the difference in the dipole moment between the ground state and the excited states. This can be analyzed by a Lippert–Mataga plot, which is essentially a plot of the Stokes shift of the fluorescence emission versus the solvent polarity [41]. The equation is expressed as followed:

$$\Delta\bar{\nu} = \bar{\nu}_a - \bar{\nu}_f = \frac{2\left(\mu_e - \mu_g\right)^2}{hca^3}\left[\frac{\varepsilon - 1}{2\varepsilon + 1} - \frac{n^2 - 1}{2n^2 + 1}\right] + \text{constant} \qquad (1a)$$

$$\Delta f = \frac{\varepsilon - 1}{2\varepsilon + 1} - \frac{n^2 - 1}{2n^2 + 1} \qquad (1b)$$

where $\bar{\nu}_a$ and $\bar{\nu}_f$ are the wavenumbers of the absorption and fluorescence maxima, $\Delta\bar{\nu}$denotes the Stokes shift, μ_g and μ_e are the ground- and excited state dipole moments respectively, ϵ and n are the dielectric constant and refractive index of the medium respectively, h is Planck's constant, c is the velocity of light, and a is the radius of the solvent cavity in which the fluorophore resides (Onsager cavity radius). The symbol Δf is called the orientation polarizability and accounts for the spectral shifts due to reorientation of the solvent molecules. In general, the reorientation of the solvent molecules is expected to result in substantial Stokes shifts.

The Lippert–Mataga plot of **3c** is depicted in Fig. 2. Twelve solvents were used to explore the change in dipole moment on excitation and poor linearity was found for the overall regression (correlation coefficient is 0.858). This is because the Lippert–Mataga equation only partially explains the effect of solvent polarity, and does not account for other effects such as hydrogen bonding to the fluorophore or internal charge transfer [42]. In **3c** the interactions between the solvent and fluorophore must be complex. *p*-Dioxane (#4) was not considered in the fitting because correlation with this solvent is usually very poor. *p*-Dioxane is known for its anomalous behavior in different polarity scales [43,44].

Quantum calculations were used to calculate the farthest distance between the carbonyl oxygen and the amino nitrogen. An Onsager cavity radius of 3.648 Å was obtained for **3c** and the dipole moment change on excitation was estimated to be around 4.31 D. This is much bigger than the values reported for PNI (3.8 D) and BNI (4.1 D) [22,25].

TD-DFT has proven to be suitable for calculating electronic excitation energies [45–48]. In order to further support our hypothesis, quantum calculation was used to analyze the photophysical properties of the 1,8-naphthalimides derivatives mentioned above.

To validate the computational method, the calculated electronic absorption and emission maxima of **3c** in the gas phase were compared with those obtained experimentally (Table 2). Although the calculated emission spectrum is blue shifted, this deviation is expected because the computations were performed without corrections for solvent effects. The calculated result for the gas phase (387 nm) correlates well with the experimental absorption maximum in cyclohexane which has quite a low polarity (389 nm). The calculated molecular structure and the electron distribution of the HOMO and LUMO of **3c** are shown in Fig. 3. Comparison of the electron distribution in the frontier molecular orbits (MOs) reveals

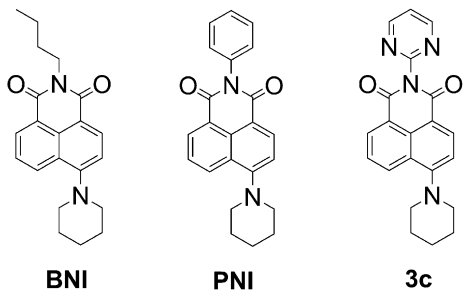

Fig. 1. 4-(1-Piperidyl)-1,8-naphthalimides derivatives with different N substituted groups.

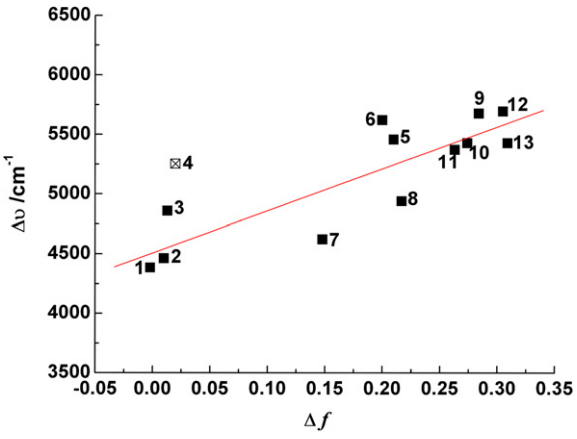

Fig. 2. Dependence of the Stokes shift $\Delta\bar{\nu}$ of **3c** on the solvent polarity function Δf. The solvents are numbered according to the sequence presented in Table 1. The straight line represents the best least-squares fit to the data (excluding the value obtained for *p*-dioxane, 4).

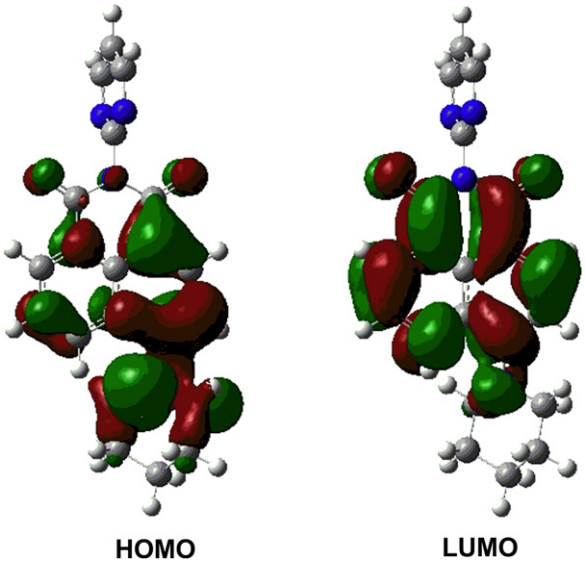

Fig. 3. Frontier orbitals of compounds **3c** calculated by the B3LYP/6-31G* DFT method.

that the HOMO–LUMO excitation shifts the electron distribution from the piperidyl moiety to the imide one. This strong migration of intramolecular charge-transfer character in these naphthalimide derivatives was also proved by Nandhikonda et al. [49]. Though the 2-pyrimidinyl group is nearly orthogonal to the naphthalimide ring, the electron density of **3c** shifts more completely to the imide moiety, suggesting the strong electron withdrawing effect of the pyrimidine moiety. The redistribution of the electron density during the HOMO–LUMO electron transition determines the influence on the photophysical properties of the dyes, such as the effect of substituents and interactions of the dye molecules with their environment.

The dipole moments μ for the ground and excited states of the 1,8-naphthalimide derivatives were also calculated in the gas phase (Table 3). For compounds **BNI**, **PNI** and **3c**, the dipole moment in the ground state ranges from 4.10–5.97 D and the difference between the dipole moments ($\Delta\mu$) of the first excited state and the ground states ranges from 1.28–1.61 D. These calculations indicate that these compounds have larger dipole moments in the excited state, which explains the experimental observations that the compounds show a bathochromic shift of their fluorescence maxima in polar solvents and that their Stokes shift in polar solvents are much larger than those in nonpolar solvents. The dipole moment change of **3c** ($\Delta\mu$ = 1.6129 D) is the largest, which also demonstrated its high sensitivity to the polarity of its surrounding solvent.

3.3. Spectral changes induced by addition of water content in organic solvents

Since the fluorescence intensity of **3c** is highly sensitive to its surroundings, it is reasonable to use it as a polarity probe. Yuan and Brown reported that the nonradiative deactivation of the fluorescent state of 4-aminonaphthalimide is quite efficient in aqueous solution, which can be attributed to the formation of a hydrogen-bonded cluster between the probe and the water molecules [23]. This fact was employed in the design of the fluorescent dye **3c** as an efficient water sensor.

The absorption and fluorescence intensities of **3c** related to the water content in a series of common solvents, such as *p*-dioxane, THF (tetrahydrofuran), acetone, DMF (dimethylformamide), acetonitrile and methanol was systematically investigated. The absorption spectra of **3c** in 0 to 10% (v/v) water spiked *p*-dioxane are shown in Fig. 4(A). When the water content is below 5% (v/v), no significant changes are seen, but when the water content is increased to above 5% (v/v), a small positive solvatochromic shift is observed. The fluorescence emission spectra of **3c** in *p*-dioxane are shown in Fig. 4(B). The spectra exhibit significant fluorescence quenching with a small red shift in the emission maxima as the water content increases. Particularly, the most dramatic changes were observed within low water concentration range of less than 5%, which spans 86% of the total changes in fluorescence intensity observed at 510 nm.

Similar results were observed for other solvents (THF, acetone, DMF, acetonitrile and methanol) (Fig. S2–S6). It should be pointed

Table 3
Calculated dipole moment (Debye) for ground (μ_g) and excited (μ_e) states of the 1,8-naphthalimide derivatives in gas phase.

Compound	μ_g	μ_e	$\Delta\mu$
BNI	5.9162	7.3267	1.4105
PNI	5.9678	7.2515	1.2837
3c	4.1026	5.7155	1.6129

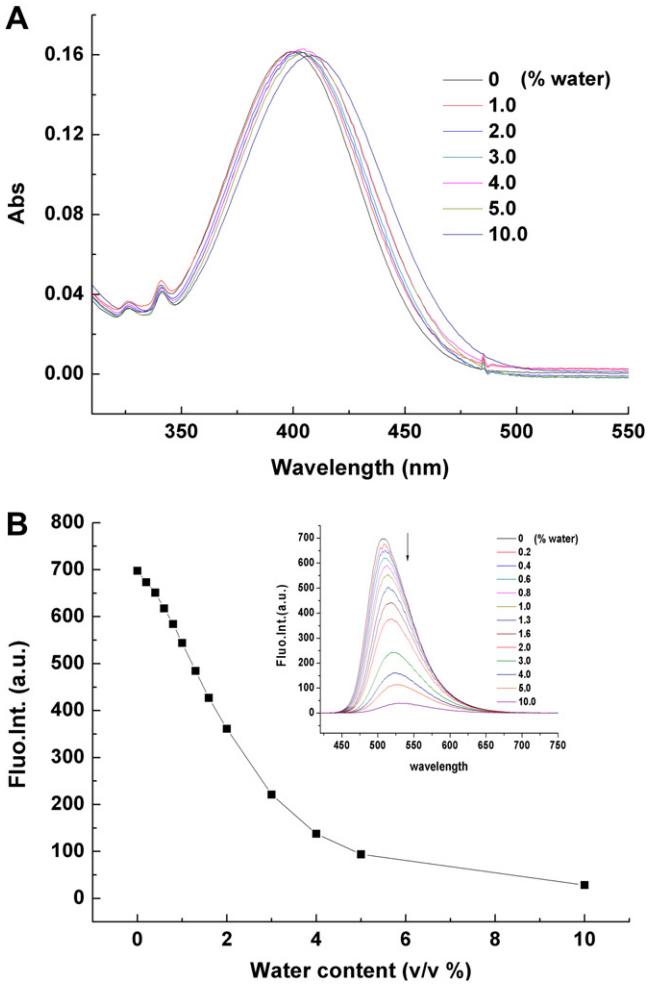

Fig. 4. (A) The profile for the absorption spectra as a function of water content in *p*-dioxane solution. (B) Changes in the fluorescence intensity at 510 nm as a function of water content, λ_{ex} = 400 nm. Inset shows the profile for the fluorescence spectra as a function of water content. [**3c**] = 1.0 × 10^{-5} mol L^{-1}.

out that the fluorescence intensities of **3c** in DMF and methanol are less sensitive to water. The addition of 50% water induces only about a 74% or 48% decreases in fluorescence intensities, respectively, and relatively larger red shifts are observed in the absorption spectra (20 nm for DMF, 14 nm for methanol).

3.4. Quantification using Stern–Volmer equation

The quenching of fluorescence of the investigated fluorophores due to the presence of water in organic solvents can be described by the Stern–Volmer equation [12,16,41].

$$\frac{F_0}{F} = 1 + K_{SV}[Q] \quad (2)$$

where F_0 and F are the fluorescence intensities in the absence and presence of the quencher, respectively, K_{SV} is the S–V quenching constant and [Q] is the quencher concentration.

When a Stern–Volmer plot was obtained using F_0/F versus [H_2O] for **3c** in *p*-dioxane, it was found to be non-linear, showing positive curvature as shown in Fig. 5A. Similar experimental results were also obtained for other solvents (Fig. S7–S11). The positive curvature from linearity suggests that quenching is not only due to collisions, but also is related to the role of a static quenching process, which has been discussed using the ground state complex or the sphere of action static quenching models [41,50–54]. Since the absorption spectra of **3c** in all of the above solvents show no observable differences in shape or maxima in both the absence and presence of water, the sphere of action static quenching model was used.

In this model [41,50–53], any static quenching interactions require that the chromophore and the quencher are within a certain distance of each another. In solution, this reaction distance defines an interaction sphere of volume V. On excitation of the chromophore, a quencher molecule which is already within this volume will be able to quench the fluorescence without the need for a diffusion controlled collisional interaction [55]. The probability of the quencher being within this volume at the time of excitation depends on the volume (V) and on the quencher concentration. Assuming the quencher is randomly distributed in solution, the probability of static quenching is given by a Poisson distribution [$e^{V[Q]}$] and the Stern–Volmer equation is modified to:

$$\frac{F_0}{F} = (1 + K_{SV}[Q])\, e^{V[Q]} \quad (3)$$

where V is the static quenching constant and represents an active volume element surrounding the excited solute molecule.

By employing Eq. (3) to fit the experimental data and using a non-linear least-squares procedure, K_{SV} and V have been determined. The best fits are shown in Fig. 5A and Fig. S7–S11 ($R^2 > 0.99$), and the results are listed in Table 4. This can serve as the basis for the quantitative determination of water in the tested organic solvents over a wide range.

It is obvious that the static quenching constants (V) are generally much smaller than the dynamic quenching constants (K_{SV}), which explains the lack of absorption spectral change with the addition of H_2O [50]. Such a weak association suggests that the fluorophores and quenchers do not actually form a ground-state complex. Therefore, it is proved that the sphere of action model is the best model for **3c**. The quenching constant K_{SV} was used to measure the sensitivity of the method, and the sensor in THF gave the highest sensitivity to water ($K_{SV} = 2.069$ L mol^{-1}).

It has been reported that at low-level concentrations of water, the fluorescence quenching of the sensor due to the presence of water fit the Stern–Volmer equation quite well [12,16]. Similar results were found in these experiments; the water sensor showed a good linear relationship between F_0/F and the water content at low concentrations (Fig. 5B and Fig. S7–S11). The detection limit was determined from 3 times the standard deviation of the blank noise (95% confidence level, $k = 3$, $n = 5$), and it was calculated to be 0.016% for acetone and 0.291% for methanol. The relative standard deviation for the determination of water concentration from the calibration curve is less than 0.08%.

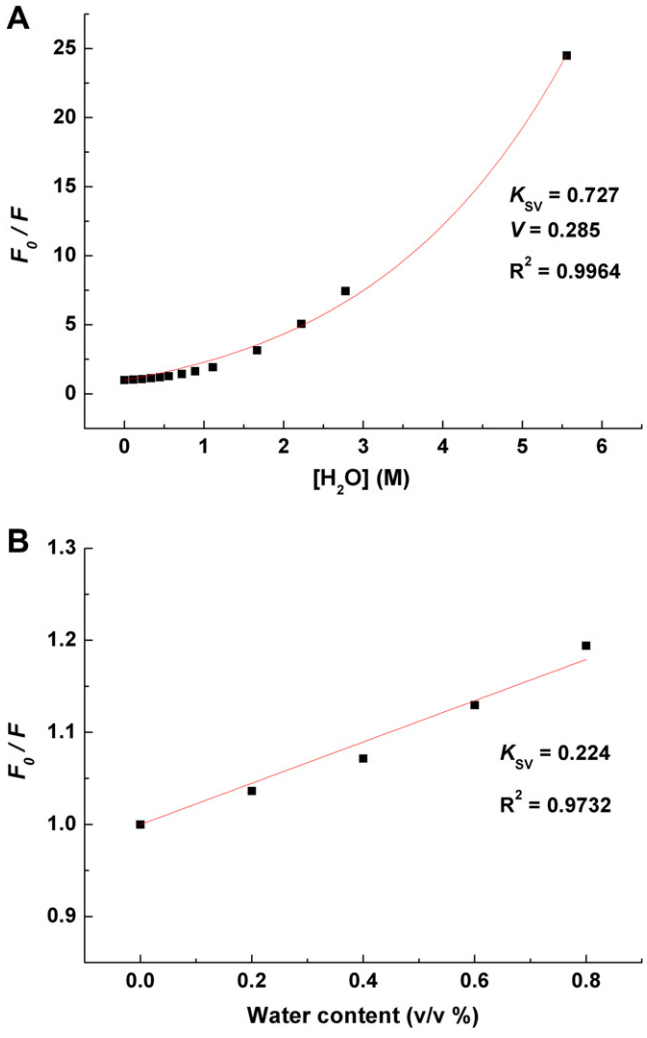

Fig. 5. (A) Modified Stern–Volmer plot for the changes in fluorescence intensity of **3c** at 510 nm as a function of water content in *p*-dioxane solution. The red line represents the best non-linear least-squares fit to the data. (B) The Stern–Volmer plot of F_0/F versus [H_2O] in *p*-dioxane with a low-level of water. [**3c**] = 1.0×10^{-5} mol L^{-1}.

Table 4
Fluorescence quenching parameters and detection limits for the fluorescent signaling of water content in organic solvents[a].

Solvent	K_{SV} (L mol^{-1})	V (L mol^{-1})	R^2	Response range	Detection limit (%)
p-Dioxane	0.7271 ± 0.1070	0.2851 ± 0.0218	0.9964	0–10%	0.049
THF	2.0691 ± 0.1864	0.1226 ± 0.0163	0.9930	0–10%	0.020
Acetone	0.9934 ± 0.0318	0.0064 ± 0.0057	0.9982	0–10%	0.016
DMF	0.0483 ± 0.0056	0.0173 ± 0.0026	0.9982	0–50%	0.054
Acetonitrile	0.8521 ± 0.0116	0.0005 ± 0.0023	0.9998	0–10%	0.021
Methanol	0.0282 ± 0.0042	0.0024 ± 0.0025	0.9977	0–50%	0.291

[a] [**3c**] = 1.0×10^{-5} mol L^{-1}.

4. Conclusions

Three 1,8-naphthalimides containing electron withdrawing *N*-heteroaryl groups have been synthesized in excellent yields under the promotion of $AlCl_3/Et_3N$ pair. It was found that the fluorescence intensity of 4-(1-piperidyl)-*N*-(2-pyrimidinyl)-1,8-naphthalimide (**3c**) is strongly affected by solvent polarity. Both experiments and theoretical calculations suggest that the introduction of a strong electron acceptor fragment to 1,8-naphthalimide significantly increased the sensitivity of **3c** to solvent polarity. This highest polar sensitivity of **3c** makes it an effective fluorescence water sensor. When **3c** was used to determine the water content in six common solvents (*p*-dioxane, THF, acetone, DMF, acetonitrile and methanol), the changes of fluorescence intensity fit quiet well with a modified Stern–Volmer equation as a function of water content. The lowest detection limit of water in *p*-dioxane, THF, acetone, and acetonitrile are 0.049, 0.020, 0.016 and 0.021%, respectively, which offers an express and suitable method for water detection of organic solvents.

Acknowledgement

The authors are grateful for the financial support of the Key Program of National Natural Science Foundation of China (No: 20834002).

Appendix. Supplementary data

Supplementary data associated with this article can be found in the online version, at doi:10.1016/j.dyepig.2010.07.009.

References

[1] Chang Q, Murtaza Z, Lakowicz JR, Rao G. A fluorescence lifetime-based solid sensor for water. Analytica Chimica Acta 1997;350(1–2):97–104.
[2] Glenn SJ, Cullum BM, Nair RB, Nivens DA, Murphy CJ, Angel SM. Lifetime-based fiber-optic water sensor using a luminescent complex in a lithium-treated Nafion™ membrane. Analytica Chimica Acta 2001;448(1–2):1–8.
[3] Liang YY. Automation of Karl Fischer water titration by flow injection sampling. Analytical Chemistry 1990;62(22):2504–6.
[4] Oraedd C, Cedergren A. Coulometric study of recovery rates for Karl Fischer titration of water in aldehydes and ketones using rapidly reacting methanolic and 2-methoxyethanolic reagents. Analytical Chemistry 1995;67(5):999–1004.
[5] Oguchi R, Yamaguchi K, Shibamoto T. Determination of water content in common organic solvents by a gas chromatograph equipped with a megabore fused-silica column and a thermal conductivity detector. Journal of Chromatographic Science 1988;26(11):588–90.
[6] Casalbore-Miceli G, Chen YS, Girotto EM, Li Y, Rinaldi AW, Yang MJ, et al. Prompt responsive sensors for water detection in organic solvents. Sensors and Actuators B: Chemical 2006;119(2):577–82.
[7] Casalbore-Miceli G, Zanelli A, Rinaldi AW, Girotto EM, Yang MJ, Chen YS, et al. A model of polyelectrolyte conductance in moist solvents as a basis of water sensors. Langmuir 2005;21(21):9704–8.
[8] Huang H, Dasgupta PK. Amperometric microsensor for water. Analytical Chemistry 1990;62(18):1935–42.
[9] Shim YB, Park JH. Humidity sensor using chemically synthesized poly(1,5-diaminonaphthalene) doped with carbon. Journal of the Electrochemical Society 2000;147(1):381–5.
[10] Liu W, Wang Y, Jin W, Shen G, Yu R. Solvatochromogenic flavone dyes for the detection of water in acetone. Analytica Chimica Acta 1999;383(3):299–307.
[11] Cho S, Chung H, Woo YA, Kim HJ. Determination of water content in ethanol by miniaturized near-infrared (NIR) system. Bulletin of the Korean Chemical Society 2005;26(1):115–8.
[12] Citterio D, Minamihashi K, Kuniyoshi Y, Hisamoto H, Sasaki S-i, Suzuki K. Optical determination of low-level water concentrations in organic solvents using fluorescent acridinyl dyes and dye-immobilized polymer membranes. Analytical Chemistry 2001;73(21):5339–45.
[13] Niu CG, Guan AL, Zeng GM, Liu YG, Li ZW. Fluorescence water sensor based on covalent immobilization of chalcone derivative. Analytica Chimica Acta 2006;577(2):264–70.
[14] Ooyama Y, Egawa H, Yoshida K. The design of a novel fluorescent PET sensor for proton and water: A phenylaminonaphtho[1,2-d]oxazol-2-yl-type fluorophore containing proton donor and acceptor groups. Dyes and Pigments 2009;82(1):58–64.
[15] Ooyama Y, Egawa H, Yoshida K. A new class of fluorescent dye for sensing water in organic solvents by photo-induced electron transfer – A (phenylamino)naphtho[1,2-d]oxazol-2-yl-type fluorophore with both proton-binding and proton-donating sites. European Journal of Organic Chemistry 2008;2008(31):5239–43.
[16] Kim JS, Choi MG, Huh Y, Kim MH, Kim SH, Wang SY, et al. Determination of water content in aprotic organic solvents using 8-hydroxyquinoline based fluorescent probe. Bulletin of the Korean Chemical Society 2006;27(12):2058–60.
[17] Choi MG, Kim MH, Kim HJ, Park JE, Chang SK. A simple ratiometric probe system for the determination of water content in organic solvents. Bulletin of the Korean Chemical Society 2007;28(10):1818–20.
[18] Kim KN, Song KC, Noh JH, Chang SK. A simple phenol-indole dye as a chromogenic probe for the ratiometric determination of water content in organic solvents. Bulletin of the Korean Chemical Society 2009;30(1):197–200.
[19] Gao F, Luo F, Chen X, Yao W, Yin J, Yao Z, et al. Fluorometric determination of water in organic solvents using europium ion-based luminescent nanospheres. Microchimica Acta 2009;166(1):163–7.
[20] Li SH, Chen FR, Zhou YF, Xu JG. $Pb_4Br_{11}^{3-}$ cluster as a fluorescent indicator for micro water content in aprotic organic solvents. The Analyst 2009;134(3):443–6.
[21] Nakaya K-i, Funabiki K, Muramatsu H, Shibata K, Matsui M. N-Aryl-1,8-naphthalimides as highly sensitive fluorescent labeling reagents for carnitine. Dyes and Pigments 1999;43(3):235–9.
[22] Saha S, Samanta A. Influence of the structure of the amino group and polarity of the medium on the photophysical behavior of 4-amino-1,8-naphthalimide derivatives. The Journal of Physical Chemistry A 2002;106(18):4763–71.
[23] Yuan D, Brown RG. Enhanced nonradiative decay in aqueous solutions of aminonaphthalimide derivatives via water-cluster formation. The Journal of Physical Chemistry A 1997;101(19):3461–6.
[24] Dmitruk S, Druzhinin S, Minakova R, Bedrik A, Uzhinov B. Radiationless deactivation of excited molecules of 4-aminonaphthalimides. Russian Chemical Bulletin 1997;46(12):2027–31.
[25] Mednykh YA, Manaev YA, Volchkov VV, Uzhinov BM. Influence of the configuration of the amine nitrogen atom on the efficiency of fluorescence of 4-aminonaphthalimide derivatives. Russian Journal of General Chemistry 2004;74(11):1728–33.
[26] Niu CG, Li LM, Qin PZ, Zeng GM, Zhang Y. Determination of water content in organic solvents by naphthalimide derivative fluorescent probe. Analytical Sciences 2010;26(6):671–4.
[27] Niu CG, Qin PZ, Zeng GM, Gui XQ, Guan AL. Fluorescence sensor for water in organic solvents prepared from covalent immobilization of 4-morpholinyl-1,8-naphthalimide. Analytical and Bioanalytical Chemistry 2007;387(3):1067–74.
[28] Li ZZ, Niu CG, Zeng GM, Qin PZ. Fluorescence sensor for water content in organic solvents based on covalent immobilization of benzothioxanthene. Chemistry Letters 2009;38(7):698–9.
[29] Crosby GA, Demas JN. Measurement of photoluminescence quantum yields. Review. The Journal of Physical Chemistry 1971;75(8):991–1024.
[30] Stephens PJ, Devlin FJ, Chabalowski CF, Frisch MJ. Ab initio calculation of vibrational absorption and circular dichroism spectra using density functional force fields. The Journal of Physical Chemistry 1994;98(45):11623–7.
[31] Miehlich B, Savin A, Stoll H, Preuss H. Results obtained with the correlation energy density functionals of becke and Lee, Yang and Parr. Chemical Physics Letters 1989;157(3):200–6.
[32] Lee C, Yang W, Parr RG. Development of the Colle-Salvetti correlation-energy formula into a functional of the electron density. Physical Review B 1988;37(2):785–9.
[33] Becke AD. Density-functional thermochemistry. III. The role of exact exchange. Journal of Chemical Physics 1993;98(7):5648–52.
[34] Foresman JB, Head-Gordon M, Pople JA, Frisch MJ. Toward a systematic molecular orbital theory for excited states. The Journal of Physical Chemistry 1992;96(1):135–49.
[35] Casida ME, Jamorski C, Casida KC, Salahub DR. Molecular excitation energies to high-lying bound states from time-dependent density-functional response theory: characterization and correction of the time-dependent local density approximation ionization threshold. Journal of Chemical Physics 1998;108(11):4439–49.
[36] Stratmann RE, Scuseria GE, Frisch MJ. An efficient implementation of time-dependent density-functional theory for the calculation of excitation energies of large molecules. Journal of Chemical Physics 1998;109(19):8218–24.
[37] Bauernschmitt R, Ahlrichs R. Treatment of electronic excitations within the adiabatic approximation of time dependent density functional theory. Chemical Physics Letters 1996;256(4-5):454–64.
[38] Frisch MJ, Trucks GW, Schlegel HB, Scuseria GE, Robb MA, Cheeseman JR, et al. Gaussian 03, revision B.05. Pittsburgh PA: Gaussian, Inc; 2003.
[39] Cao H, Chang V, Hernandez R, Heagy MD. Matrix screening of substituted *N*-aryl-1,8-naphthalimides reveals new dual fluorescent dyes and unusually bright pyridine derivatives. The Journal of Organic Chemistry 2005;70(13):4929–34.
[40] Reichardt C. Solvatochromic dyes as solvent polarity indicators. Chemical Reviews 1994;94(8):2319–58.
[41] Lakowicz JR. Principles of fluorescence spectroscopy. 3rd ed. New York: Springer Berlin/Heidelberg Publishers; 2006.

[42] Reichardt C. Solvents and solvent effects in organic chemistry. 3rd ed. Weinheim, Germany: Wiley-VCH; 2003.
[43] Dong DC, Winnik MA. The Py scale of solvent polarities. Canadian Journal of Chemistry 1984;62(11):2560–5.
[44] Seth D, Sarkar S, Pramanik R, Ghatak C, Setua P, Sarkar N. Photophysical studies of a hemicyanine dye (LDS-698) in dioxane-water mixture, in different alcohols, and in a room temperature ionic liquid. The Journal of Physical Chemistry B 2009;113(19):6826–33.
[45] Scholz R, Kobitski AY, Zahn DRT, Schreiber M. Investigation of molecular dimers in α-PTCDA by ab initio methods: Binding energies, gas-to-crystal shift, and self-trapped excitons. Physical Review B 2005;72(24):245208–25.
[46] Neiss C, Saalfrank P, Parac M, Grimme S. Quantum chemical calculation of excited states of flavin-related molecules. The Journal of Physical Chemistry A 2003;107(1):140–7.
[47] Jodicke CJ, Luthi HP. Time-dependent density-functional theory investigation of the formation of the charge transfer excited state for a series of aromatic donor-acceptor systems. Part I. Journal of Chemical Physics 2002;117 (9):4146–56.
[48] Adamo C, Barone V. A TDDFT study of the electronic spectrum of s-tetrazine in the gas-phase and in aqueous solution. Chemical Physics Letters 2000;330(1-2):152–60.
[49] Nandhikonda P, Paudel S, Heagy MD. Minimal modification approach to red-shifted absorption and fluorescence in 1,8-naphthalimides. Tetrahedron 2009;65(11):2173–7.
[50] Behera PK, Mukherjee T, Mishra AK. Simultaneous presence of static and dynamic component in the fluorescence quenching for substituted naphthalene-CCl_4 system. Journal of Luminescence 1995;65(3):131–6.
[51] Zeng H, Durocher G. Analysis of fluorescence quenching in some antioxidants from non-linear Stern-Volmer plots. Journal of Luminescence 1995;63(1-2):75–84.
[52] Hanagodimath SM, Evale BG, Manohara SR. Nonlinear fluorescence quenching of newly synthesized coumarin derivative by aniline in binary mixtures. Spectrochimica Acta Part A: Molecular and Biomolecular Spectroscopy 2009;74(4):943–8.
[53] Giri R. Fluorescence quenching of coumarins by halide ions. Spectrochimica Acta Part A: Molecular and Biomolecular Spectroscopy 2004;60(4):757–63.
[54] Kumar Behera P, Kumar Mishra A. Static and dynamic model for 1-naphthol fluorescence quenching by carbon tetrachloride in dioxane-acetonitrile mixtures. Journal of Photochemistry and Photobiology A: Chemistry 1993;71 (2):115–8.
[55] Eftink MR, Ghiron CA. Fluorescence quenching studies with proteins. Analytical Biochemistry 1981;114(2):199–227.